The following publication S. Zhang, M. Zhang and S. W. Or, "Bidirectional Current–Voltage Converter Based on Coil-Wound, Intermagnetically Biased, Heterostructured Magnetoelectric Ring," in IEEE Transactions on Magnetics, vol. 52, no. 7, pp. 1-5, July 2016 is available at https://doi.org/10.1109/TMAG.2016.2523558

Bidirectional Current–Voltage Converter Based on Coil-Wound, Intermagnetically Biased, Heterostructured Magnetoelectric Ring

Shengyao Zhang, Mingji Zhang, and Siu Wing Or

Department of Electrical Engineering, The Hong Kong Polytechnic University, Hong Kong

We report theoretically and experimentally a passive bidirectional current–voltage (*I–V*) converter, capable of converting input currents into output voltages, and conversely, input voltages into output currents, based on a multiphase heterostructured magnetoelectric (ME) ring. The ME ring has a coil-wound, intermagnetically biased magnetostrictive–piezoelectric heterostructure in which an axially polarized PZT piezoelectric ceramic ring is bonded between two circumferentially magnetized, intermagnetically biased Terfenol-D short-fiber/NdFeB magnet/epoxy three-phase magnetostrictive composite rings. In *I–V* conversion, a current applied to the coil induces a vortex magnetic field to the ME ring, resulting in an open-circuit voltage from the ME ring because of the direct ME effect. In *V–I* conversion, a voltage applied to the ME ring produces a circumferential magnetic induction due to the converse ME effect, leading to a short-circuit current from the coil. The converter exhibits simultaneously large *I–V* and *V–I* conversion factors of ~0.3 V/A and ~0.2 mA/V in a broad non-resonance frequency range up to 80 kHz as well as enhanced conversion factors of ~7 and ~25 times at the resonance frequency of 122 kHz, respectively.

***Index Terms*—Bidirectional current–voltage (*I–V*) converter, magnetostrictive–piezoelectric heterostructure, magnetoelectric ring.**

I. Introduction

CURRENT–voltage (*I–V*) and voltage–current (*V–I*) converters are fundamental devices or modules for electrical and electronic circuits and systems to covert input currents into output voltages and input voltages into output currents, respectively [1]. Traditional *I–V* and *V–I* converters are best represented by operational amplifier-based electronic converters. While featuring high designability and wide applicability, these active-type electronic converters are generally limited by unidirectional *I–V* or *V–I* conversion and the need of external power supplies to sustain their operations.

The recent development of magnetoelectric (ME) materials enables novel electromagnetic devices. In fact, ME materials can generate an electric field or voltage when they are exposed to an applied magnetic field on the basis of the direct ME effect. Conversely, they can produce a magnetic induction when they are driven by an electric field or voltage in the light of the converse ME effect. Over the past decade, considerable reports have been published using the direct ME effect to realize power supply-free passive magnetic field and electric current sensors as well as employing the converse ME effect to actualize coil-free electromagnetic actuators [2]–[7].

By properly utilizing and combining the direct and converse ME effects with the basic laws of electromagnetism (i.e., Ampère's and Faraday's laws) in a specifically designed multiphase heterostructured ME ring, we have developed a passive-type bidirectional *I–V* converter, featuring simultaneously large *I–V* and *V–I* conversion factors of ~0.3 V/A and ~0.2 mA/V over a broad range of non-resonance frequencies up to 80 kHz, besides showing much larger conversion factors of ~7 and ~25 times at 122 kHz resonance, respectively. These attractive features are underpinned by an improved ability to conserve magnetic energy for conversion into electric energy via the channeling and completion of the magnetic flux path in the ME ring in comparison with the converters based on plate-shaped ME laminates [8].

Manuscript received November 6, 2015. Corresponding author: S. W. Or (e-mail: eeswor@polyu.edu.hk).

Color versions of one or more of the figures in this paper are available online at http://ieeexplore.ieee.org.

Digital Object Identifier (inserted by IEEE).

II. Structure and Working Principle

Fig. 1(a) shows the structure of proposed passive bidirectional *I–V* converter in the form of a coil-wound, intermagnetically biased, magnetostrictive–piezoelectric (MS–PE) heterostructured ME ring. The ME ring has a PZT piezoelectric ceramic ring (PECR) with an axial polarization (*P*) adhesively bonded between two Terfenol-D short-fiber/ NdFeB magnet/epoxy three-phase magnetostrictive composite rings (MSCRs) with a circumferential magnetization (*M*) and an internal magnetic biasing to form a ring-shaped, intermagnetically biased MS–PE heterostructure. The whole heterostructure is wound by an enameled copper wire of 0.2 mm diameter to give a wound coil of 50 turns (*N*) and the coil port. The two electrodes of the PECR form the ME port. The coil and ME ports function as the *I* input and *V* output ports for *I–V* conversion in Fig. 1(b), respectively. They also serve as the *I* output and *V* input ports for *V–I* conversion in Fig. 1(c). The PECR is a CeramTech P8 hard PZT with an inner radius (R_1) of 2.5 mm, an outer radius (R_2) of 5.25 mm, and a thickness (t_p) of 1 mm. The MSCRs are self-prepared with the same dimensions as the PECR. The preparation of the MSCRs has been reported elsewhere [9],[10]. The creation of the MSCRs is primarily aimed to provide a circumferential magnetization to channel and complete the vortex magnetic fields or the circumferential magnetic induction associated with both the ME effects and basic laws of electromagnetism in the ME ring in order to minimize magnetic field leakages and hence magnetic energy losses [9]. The MSCRs also enable an internal magnetic biasing so that the external magnetic biasing means as used in the plate-shaped ME laminate converters and most other ME devices is not required [8]. Other benefits include reducing eddy-current losses, widening operating frequency range, reducing mechanical brittleness, etc. when compared with Terfenol-D and its devices [9].

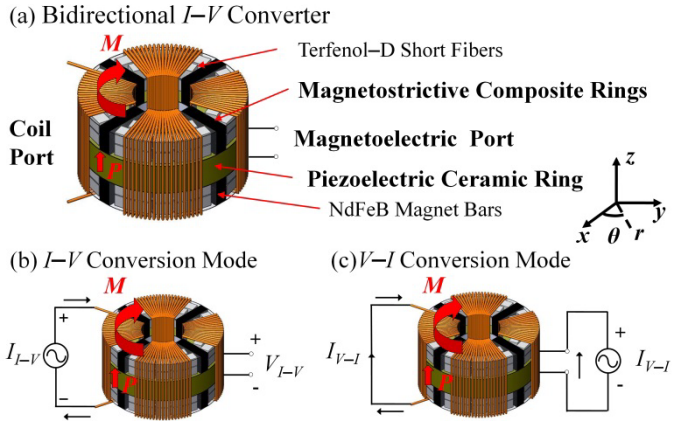

Fig. 1. (a) Structure of the proposed passive bidirectional *I–V* converter based on a coil-wound, intermagnetically biased, MS–PE heterostructured ME ring. (b) *I–V* conversion mode. (c) *V–I* conversion mode.

For *I–V* conversion in Fig. 1(b), an ac current (I_{I-V}) applied to the coil port induces an ac vortex magnetic field in the wound coil in accordance with Ampère's law. This ac vortex magnetic field causes the two MSCRs to produce radial and circumferential motions based on the direct MS effect. Due to mechanical coupling, the induced MS strains lead to stresses in the central PECR, thereby producing an ac open-circuit voltage (V_{I-V}) across the thickness of the PECR and also at the ME port based on the direct PE effect. The product of the direct MS and PE effects results in the direct ME effect which, in combination with Ampère's law, gives rise to *I–V* conversion in the ME ring. The *I–V* conversion factor (α) can be defined as

$$\alpha = \frac{dV_{I-V}}{dI_{I-V}}. \tag{1}$$

For *V–I* conversion in Fig. 1(c), an ac voltage (V_{V-I}) applied to the ME port induces radial and circumferential motions in the PECR because of the converse PE effect. These motions, owing to mechanical coupling, lead to stresses in the two outer MSCRs, causing them to produce circumferential magnetic induction as a result of the converse MS effect. This circumferential magnetic induction gives rise to a short-circuit current (I_{V-I}) in the wound coil on the basis of Faraday's law of electromagnetic induction. The product of the converse PE and MS effects results in the converse ME effect which, together with Faraday's law, leads to *V–I* conversion in the ME ring. The *V–I* conversion factor (β) is defined as

$$\beta = \frac{dI_{V-I}}{dV_{V-I}}. \tag{2}$$

III. Theoretical Analysis

For *I–V* conversion, I_{I-V} induces an ac vortex magnetic field (H_θ) in the wound coil by Ampère's law as follows:

$$H_\theta = \frac{N}{L} I_{I-V}, \tag{3}$$

where N is the number of turns of the wound coil and L is the mean circumference of the ME ring. Assuming the radial (T_r) and circumferential (T_θ) stresses are perfectly coupled at the interfaces of the MSCRs and the PECR in the ME ring, the following boundary conditions should be satisfied:

$$2T_{r,\mathrm{m}}t_\mathrm{m} + T_{r,\mathrm{p}}t_\mathrm{p} = 0 \tag{4a}$$
$$2T_{\theta,\mathrm{m}}t_\mathrm{m} + T_{\theta,\mathrm{p}}t_\mathrm{p} = 0, \tag{4b}$$

where the subscripts m and p denote the MSCRs and PECR, respectively, and t is the thickness. By substituting (3) and (4) into the constitutive equations for MS and PE materials [11],[12], the *I–V* conversion factor (α) is solved by weak-form as [13]–[15]

$$\alpha = \frac{dH_\theta}{dI_{I-V}} \cdot \frac{dV_{I-V}}{dH_\theta} = \tag{5}$$
$$\frac{N}{L}\left| \frac{\left[N^{\mathrm{EM}}_{1,I-V} \quad N^{\mathrm{EM}}_{2,I-V}\right]\begin{bmatrix}-\omega^2 M_{11}+K_{11}+j\omega\zeta K_{11} & -\omega^2 M_{12}+K_{12}+j\omega\zeta K_{12}\\ -\omega^2 M_{21}+K_{21}+j\omega\zeta K_{21} & -\omega^2 M_{22}+K_{22}+j\omega\zeta K_{22}\end{bmatrix}^{-1}\begin{bmatrix}N^{\mathrm{MM}}_{1,I-V}\\ N^{\mathrm{MM}}_{2,I-V}\end{bmatrix}}{C_{I-V}+\left[N^{\mathrm{EM}}_{1,I-V} \quad N^{\mathrm{EM}}_{2,I-V}\right]\begin{bmatrix}-\omega^2 M_{11}+K_{11}+j\omega\zeta K_{11} & -\omega^2 M_{12}+K_{12}+j\omega\zeta K_{12}\\ -\omega^2 M_{21}+K_{21}+j\omega\zeta K_{21} & -\omega^2 M_{22}+K_{22}+j\omega\zeta K_{22}\end{bmatrix}^{-1}\begin{bmatrix}N^{\mathrm{EM}}_{1,I-V}\\ N^{\mathrm{EM}}_{2,I-V}\end{bmatrix}}\right|,$$

where ω is the angular frequency and ζ is the coefficient accounting for damping effect. Other parameters are described in Table I. More details can be found in Ref. 16.

For *V–I* conversion, V_{V-I} results in an ac axial electric field (E_z) in the PECR as follows:

$$E_z = -V_{V-I}/t_\mathrm{p}. \tag{6}$$

Substituting (6) and (4) into the MS and PE constitutive equations [11],[12] and combining Faraday's law, we have

$$I_{V-I} = -j\omega N B_\theta S/Z_\mathrm{coil}, \tag{7}$$

where B_θ is the circumferential magnetic induction, S is the cross-section area of the MSCRs, and Z_coil is the internal impedance of the wound coil. The *V–I* conversion factor (β) can be solved by weak-form as [13]–[15]

$$\beta = \frac{dB_\theta}{dV_{V-I}} \cdot \frac{dI_{V-I}}{dB_\theta} = \left|\frac{\omega N S}{Z_\mathrm{coil}(R_2-R_1)}\right| \cdot \tag{8}$$
$$\left| \frac{\left[N^{\mathrm{MM}}_{1,V-I} \quad N^{\mathrm{MM}}_{2,V-I}\right]\begin{bmatrix}-\omega^2 M'_{11}+K'_{11}+j\omega\zeta K'_{11} & -\omega^2 M'_{12}+K'_{12}+j\omega\zeta K'_{12}\\ -\omega^2 M'_{21}+K'_{21}+j\omega\zeta K'_{21} & -\omega^2 M'_{22}+K'_{22}+j\omega\zeta K'_{22}\end{bmatrix}^{-1}\begin{bmatrix}N^{\mathrm{EM}}_{1,V-I}\\ N^{\mathrm{EM}}_{2,V-I}\end{bmatrix}}{C_{V-I}-\left[N^{\mathrm{MM}}_{1,V-I} \quad N^{\mathrm{MM}}_{2,V-I}\right]\begin{bmatrix}-\omega^2 M'_{11}+K'_{11}+j\omega\zeta K'_{11} & -\omega^2 M'_{12}+K'_{12}+j\omega\zeta K'_{12}\\ -\omega^2 M'_{21}+K'_{21}+j\omega\zeta K'_{21} & -\omega^2 M'_{22}+K'_{22}+j\omega\zeta K'_{22}\end{bmatrix}^{-1}\begin{bmatrix}N^{\mathrm{MM}}_{1,V-I}\\ N^{\mathrm{MM}}_{2,V-I}\end{bmatrix}}\right|.$$

Other parameters are specified in Table I and also detailed in Ref. 16.

By substituting the geometric properties described in Sections. II and III and the material properties reported in Refs. 17 and 18 into (5) and (8), the α and β spectra of the converter can be calculated, respectively. It is noted that α and β depend on the input I_{I-V} and V_{V-I}, respectively. They can be enhanced by simply increasing N.

TABLE I
Basic Parameters for Equations [16]

Symbol	Meaning	Unit
M_{ij} or M'_{ij}	Mass coefficient for *I–V* or *V–I* conversion	kg
K_{ij} or K'_{ij}	Elastic coefficient for *I–V* or *V–I* conversion	N/m
$N^{\mathrm{EM}}_{i,I-V}$	Electromechanical coupling coefficient for *I–V* conversion	N/V
$N^{\mathrm{EM}}_{i,V-I}$	Electromechanical coupling coefficient for *V–I* conversion	N/V
$N^{\mathrm{MM}}_{i,I-V}$	Magnetomechanical coupling coefficient for *I–V* conversion	N/(A/m)
$N^{\mathrm{MM}}_{i,V-I}$	Magnetomechanical coupling coefficient for *V–I* conversion	A
C_{I-V}	Polarization voltage coefficient	C/V
C_{V-I}	Magnetization current coefficient	A/T

IV. Measurements

The magnitude ($|Z_\mathrm{in}|$) and phase (θ) spectra of the input electrical impedance (Z_in) of the converter operating in *I–V* and *V–I* conversion modes and with the corresponding output

port (i.e., the ME and coil ports) short- and open-circuited were measured using an Agilent 4292A precision impedance analyzer. The input–output characteristics (i.e., the I_{I-V}–V_{I-V} and V_{V-I} – I_{V-I} responses) at different frequencies (f) were evaluated, together with the α and β spectra, using an in-house measurement system. The input signals to the converter were generated as a sinusoidal voltage of constant amplitude and at a prescribed frequency by an Agilent 33210A waveform generator. They were then amplified by an AE Techron TEC7572 supply amplifier configured in constant-current and constant-voltage modes to give an ac current (I_{I-V}) for I–V conversion and an ac voltage (V_{V-I}) for V–I conversion, respectively. The output signals from the converter, which were an ac voltage (V_{I-V}) for I–V conversion and an ac current (I_{V-I}) for V–I conversion, were monitored using a Tektronix DPO2014 digital oscilloscope. A Tektronix P2221 voltage probe was used to acquire both V_{I-V} and V_{V-I}, while a Hioki 9273 current probe connected to a Hioki 3271 signal amplifier was employed to quantify both I_{I-V} and I_{V-I}.

V. Results and Discussion

Fig. 2(a) shows the measured $|Z_{in}|$ and θ spectra of the converter operating in I–V conversion mode and with the ME port short- and open-circuited. The monotonic increase in $|Z_{in}|$ and θ toward higher $|Z_{in}|$ values and 90°, respectively, with increasing f indicates an inductive nature of the input of the converter no matter the ME port is open- or short-circuited. This, in turn, implies that the wound coil has the dominant effect on the input behavior of the I–V conversion mode. Fig. 2(b) plots the measured $|Z_{in}|$ and θ spectra of the converter operating in V–I conversion mode and with the coil port short- and open-circuited. The decrease in $|Z_{in}|$ and the presence of θ at ~-90°, both for f below ~80 kHz and above ~160 kHz, suggest a capacitive nature of the input of the converter irrespective of the open- or short-circuit of the coil port. Besides, a resonance effect is observed in the 80–160 kHz range with the resonance peak at 122 kHz. The observations elucidate that the ring-shaped, intermagnetically biased MS–PE heterostructure, the PECR in particular, is playing the dominant role in the input behavior of the V–I conversion mode, and the observed resonance peak at 122 kHz represents an electromechanical resonance of the heterostructure. It should be noted that the magnetomechanical resonance, which is expected to present in I–V conversion mode, is now unobservable in Fig. 2(a) due to the small-signal (~1 mA) driving of the wound coil by the impedance analyzer.

Figs. 3(a) and 3(b) show the measured and calculated α and β spectra for I–V and V–I conversions, respectively. The measured α and β spectra were obtained by applying an ac current of 35 mA peak to the coil port and an ac voltage of 18 V peak to the ME port at various f, respectively. The calculated α and β spectra were based on (5) and (8), respectively, using the geometric properties described in Sections II and III and the material properties reported in Refs. 17 and 18. In Fig. 3(a), the converter exhibits a very stable α value of ~0.3 V/A in a broad non-resonance f range up to ~80 kHz. This α value is greatly enhanced by ~7 times at the resonance f of 122 kHz. In Fig. 3(b), the converter, again, demonstrates a stable β value of ~0.2 mA/V in the non-resonance f range and a significant enhancement in β by ~25 times at the resonance f of 122 kHz. The measured and calculated α and β values are in good agreement with less than 10% error. It is interesting to note that the resonance α and β occur at the same f at 122 kHz. This indicates that they essentially originate from the mechanical resonance of the ME ring [2]. From the theoretical analysis in Section III, the said mechanical resonance can be described predominately by the radial and circumferential motions in the ME ring.

Figs. 4(a) and 4(b) plot the measured and calculated input–output characteristics of the converter at five different f of 1, 100, 110, 122 (resonance), and 130 kHz for I–V and V–I conversions, respectively. It is clear that the $I_{I-V} - V_{I-V}$ responses for I–V conversion and the V_{V-I}–I_{V-I} responses for V–I conversion display excellent linear input–output relationships at different f. Therefore, the converter is a linear bidirectional I–V conversion device for proportional conversion between input I or V into output V or I.

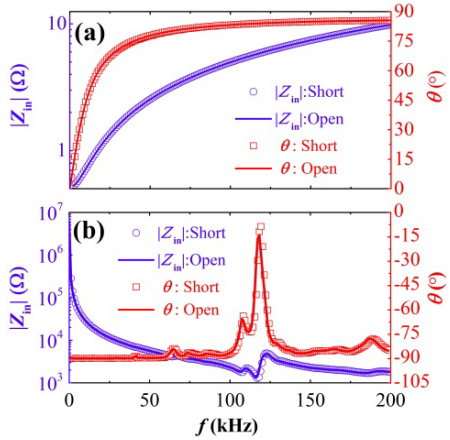

Fig. 2. Measured $|Z_{in}|$ and θ spectra of the converter operating in (a) I–V and (b) V–I conversion modes and with the output port short- and open-circuited.

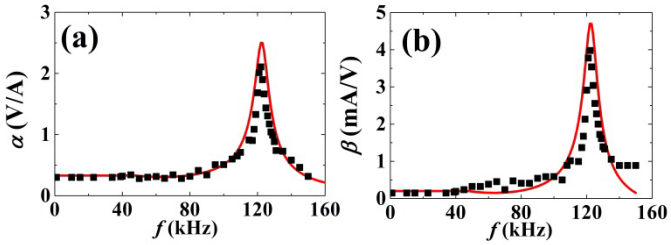

Fig. 3. Measured (symbols) and calculated (lines) (a) α spectrum for I–V conversion and (b) β spectrum for V–I conversion.

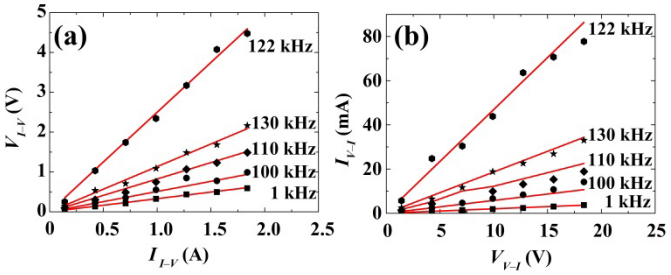

Fig. 4. Measured (symbols) and calculated (lines) input–output characteristics at different f for (a) I–V and (b) V–I conversions.

Fig. 5 shows the measured input and output waveforms for *I–V* and *V–I* conversions at 1 and 122 (resonance) kHz. For *I–V* conversion in Figs. 5(a) and 5(b), V_{I-V} (output *V*) at 122 kHz resonance is ~7 times larger than that at 1 kHz under a given I_{I-V} (input *I*). The observation coincides with that in Fig. 3(a). For *V–I* conversion in Figs. 5(c) and 5(d), I_{V-I} (output *I*) at 122 kHz resonance is ~25 times higher than that at 1 kHz under the same V_{V-I} (input *V*). This also agrees with the observation in Fig. 3(b). Moreover, I_{I-V} and V_{I-V} in *I–V* conversion at 1 kHz in Fig. 5(a) as well as V_{V-I} and I_{V-I} in *V–I* conversion at 1 kHz in Fig. 5(c) are essentially in phase, indicating a resistive nature between the input and output of the converter. At 122 kHz resonance, the existence of a 90° phase lead in V_{I-V} with respect to I_{I-V} in *I–V* conversion in Fig. 5(b) implies an inductive nature, while the presence of a 90° phase lead in I_{V-I} with respect to V_{V-I} in *V–I* conversion in Fig. 5(d) suggests a capacitive nature.

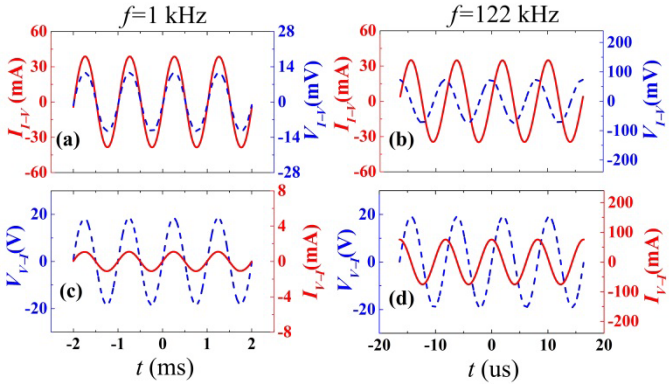

Fig. 5. Measured input and output waveforms for *I–V* conversion at (a) 1 kHz and (b) 122 kHz as well as *V–I* conversion at (c) 1 kHz and (d) 122 kHz.

VI. Conclusion

We have developed a passive bidirectional *I–V* converter based on a coil-wound, intermagnetically biased MS–PE heterostructured ME ring and evaluated theoretically and experimentally its *I–V* and *V–I* conversion principles and performance. The *I–V* conversion has been described by the product of the direct ME effect and the Ampère's law, while the *V–I* conversion has been ascribed to the product of the converse ME effect and the Faraday's law of electromagnetic induction, both in the ME ring. The converter has showed simultaneously large $\boldsymbol{\alpha}$ and $\boldsymbol{\beta}$ values of ~0.3 V/A and ~0.2 mA/V over a broad non-resonance frequency range up to 80 kHz in addition to enhanced resonance $\boldsymbol{\alpha}$ and $\boldsymbol{\beta}$ of ~7 and ~25 times at 122 kHz, respectively. Comparing to the traditional operational amplifier-based (active), unidirectional electronic *I–V* or *V–I* converters, our converter has demonstrated the distinct advantages of passive operations without the support of external power supplies as well as bidirectional *I–V* and *V–I* conversions. Comparing to the early reported plate-shaped ME laminate converters, our converter has exhibited an improved ability to minimize magnetic field leakages and hence magnetic energy losses via the channeling and completion of the magnetic flux path in the MSCRs of the ME ring. Moreover, the MSCRs have enabled internal magnetic biasing so that external magnetic biasing is not required. In addition, the problems of eddy-current losses, limited operational frequency range, mechanical brittleness, etc. intrinsic in monolithic Terfenol-D-based devices have been improved.

Acknowledgments

This work was supported by the Research Grants Council of the HKSAR Government (PolyU 5228/13E) and The Hong Kong Polytechnic University (RTUY).

References

[1] K. Gupta, B. P. Singh, and R. Choudhary, "Design and analysis of current-to-voltage and voltage-to-current converters using 0.35 μm technology," *Inter. J. Eng. Techno. Adv. Eng.*, vol. 2, pp. 457–461, 2012.
[2] Y. K. Fetisov, "Electric field tuning characteristics of a ferrite-piezoelectric microwave resonator," *Appl. Phys. Lett.*, vol. 88, article 143503, 2006.
[3] S. Priya, R. Islam, S. X. Dong, D. Viehland, "Recent advancements in magnetoelectric particulate and laminate composites," *J. Electroceram.*, vol. 19, pp. 147–164, 2007.
[4] Y. J. Wang, S. W. Or, H. L. W. Chan, X. Y. Zhao, and H. S. Luo, "Magnetoelectric effect from mechanically mediated torsional magnetic force effect in NdFeB magnets and shear piezoelectric effect in 0.7Pb($Mg_{1/3}Nb_{2/3}$)O_3–0.3$PbTiO_3$ single crystal," *Appl. Phys. Lett.*, vol. 92, article 123510, 2008.
[5] J. X. Zhang, J. Y. Dai, L. C. So, C. L. Sun, C. Y. Lo, S. W. Or, and H.L.W. Chan, "The effect of magnetic nanoparticles on the morphology, ferroelectric, and magnetoelectric behaviors of CFO/P(VDF–TrFE) 0–3 nanocomposites", *J. Appl. Phys.*, vol. 105, article 054102, 2009.
[6] Y. M. Jia, S. W. Or, H. L. W. Chan, X. Y. Zhao, and H. S. Luo, "Converse magnetoelectric effect in laminated composites of PMN–PT single crystal and Terfenol-D alloy", *Appl. Phys. Lett.*, vol. 88, article 242902, 2006.
[7] S. C. Yang, J.-H. Cho, C.-S. Park, and S. Priya, "Self-biased converse magnetoelectric effect," Appl. Phys. Lett., vol. 99, article 202904, 2011.
[8] Y. M. Jia, S. W. Or, H. L. W. Chan, J. Jiao, H. S. Luo, and S. van der Zwaag, "Bidirectional current–voltage converters based on magnetostrictive/piezoelectric composites," *Appl. Phys Lett*., vol. 94, article 263504, 2009.
[9] C. M. Leung, S. W. Or, S. Y. Zhang, and S. L. Ho, "Ring-type electric current sensor based on ring-shaped magnetoelectric laminate of epoxy-bonded $Tb_{0.3}Dy_{0.7}Fe_{1.92}$ short-fiber/NdFeB magnet magnetostrictive composite and Pb(Zr, Ti)O_3 piezoelectric ceramic," *J. Appl. Phys.*, vol. 107, article 09D918, 2010.
[10] S. Y. Zhang, C. M. Leung, W. Kuang, S. W. Or, and S. L. Ho, "Concurrent operational modes and enhanced current sensitivity in heterostructure of magnetoelectric ring and piezoelectric transformer," *J. Appl. Phys*., vol. 113, article 17C733, 2013.
[11] G. Engdahl, *Magnetostrictive Materials Handbook*, Academic, New York, 2000.
[12] T. Ikeda, *Fundamentals of Piezoelectricity*, Oxford University Press, Oxford, 1990.
[13] S. T. Ho, "Electromechanical analysis of a ring-type piezoelectric transformer," in *Mechatronic Systems Simulation Modeling and Control*, chapter 1, A. M. Donato Di Paola and G. Cicirelli, Eds. Intech, 2010, pp. 1–16.
[14] Z. Ren, B. Ionescu, M. Besbes, and A. Razek, "Calculation of mechanical deformation of magnetic materials in electromagnetic devices," *IEEE Trans. Magn*., vol. 31, pp. 1873–1876, 1995.
[15] F. Claeyssen, N. Lhermet, R. Le Letty, and P. Bouchilloux, "Actuators, transducers and motors based on giant magnetostrictive materials," *J. Alloy Compd*., vol. 258, pp. 61–72, 1997.
[16] S. Y. Zhang, *Development of Ring-type Electric Current Sensors for Condition Monitoring Applications*, Ph.D. Thesis, The Hong Kong Polytechnic University, Hong Kong, 2016, unpublished.
[17] S. W. Or and G. P. Carman, "Dynamic magnetoelastic properties of epoxy-bonded Terfenol-D particulate composite with a preferred [112] crystallographic orientation," *IEEE Trans. Magn*., vol. 41, pp. 2790–2792, 2005.
[18] www.piezo-kinetics.com, last access: Jan, 2016.